Supplementary Material for "Rain Streaks Removal From Light Field Images"

Yuyang Ding, Mingyue Li, Tao Yan*, Fan Zhang, Yuan Liu, Rynson H.W. Lau

Tabs. I- III show details of our proposed network architecture. Tabs. IV and V show the PSNR and SSIM values of all comparison experimental results.

Figs. 1- 5 show supplementary experimental results. Figs. 6- 7 and 8 show the depth maps and rain-streak images produced by our method and method [1] for the synthetic and real-world LFIs exhibited in our paper, respectively. Fig. 9 shows the comparison of rain removal by taking different methods, our method and the methods [1] [2] [3], on real-world LFIs. Figs. 10 and 11 show some selected de-rained subaperture views of the rainy LFIs produced by our method and methods [4] [5].

Fig. 12 shows the correlation of rain streaks from different sub-viewpoints in the real scene, and dashed lines indicate the coordiantes of rain streaks in different sub-views.

Layer	Parameter
Input	num_c=3
Conv1	3x3x3, num_c=32
Dilated_Conv1	3x3x3, num_c=32
Max_P1	2x2x1, num_c=32
Conv2	3x3x3, num_c=64
Dilated_Conv2	3x3x3, num_c=64
Max_P2	2x2x1, num_c=64
Conv3	3x3x3, num_c=128
Dilated_Conv3	3x3x3, num_c=128
Max_P3	2x2x1, num_c=128
FC	num_c=128
Output	num_c=128

TABLE I: Parameters in architectural of our proposed *Discriminator 1* and *Discriminator 2*.

Layer	Parameter
Input	num_c=3
Conv1	3x3x3, num_c=32
Non-Local	num_c=32
Conv2	3x3x3, num_c=64
Max_P1	2x2x1, num_c=64
Conv3	3x3x3, num_c=128
Max_P2	2x2x1, num_c=128
Conv4	3x3x3, num_c=256
Max_P3	2x2x1, num_c=256
Conv5	3x3x3, num_c=512
Up_P1	2x2x1, num_c=512
Conv6	3x3x3, num_c=256
Up_P2	2x2x1, num_c=256
Conv7	3x3x3, num_c=128
Up_P3	2x2x1, num_c=64
Conv8	3x3x3, num_c=64
Conv9	3x3x3, num_c=16
Conv10	3x3x3, num_c=1
Output	num_c=1

TABLE II: Parameters in architectural of the Disparity Estimation Network (DE-Net).

Layer	Parameter
Input	num_c=4
Conv1	3x3x3, num_c=32
Contextual	num_c=96
Conv2	3x3x3, num_c=64
Max_P1	2x2x1, num_c=64
Conv3	3x3x3, num_c=128
Max_P2	2x2x1, num_c=128
Conv4	3x3x3, num_c=256
Max_P3	2x2x1, num_c=256
Conv5	3x3x3, num_c=512
Conv6	3x3x3, num_c=1024
Up_P1	2x2x1, num_c=512
Conv7	3x3x3, num_c=256
Up_P2	2x2x1, num_c=256
Conv8	3x3x3, num_c=128
Up_P3	2x2x1, num_c=64
Conv9	3x3x3, num_c=64
Conv10	3x3x3, num_c=16
Conv11	3x3x3, num_c=1
Output	num_c=3

TABLE III: Parameters in architectural of the U-shaped Background Recovery Network(BR-Net).

References

[1] R. Li, L. Cheong, and R. T. Tan, "Heavy rain image restoration: Integrating physics model and conditional adversarial learning," in *Proc. IEEE CVPR*, 2019.

[2] T. Wang, X. Yang, K. Xu, S. Chen, Q. Zhang, and R. W. Lau, "Spatial attentive single-image deraining with a high quality real rain dataset," in *Proc. IEEE CVPR*, 2019.

[3] K. Jiang, Z. Wang, P. Yi, C. Chen, B. Huang, Y. Luo, J. Ma, and J. Jiang, "Multi-scale progressive fusion network for single image deraining," in *Proc. IEEE CVPR*, 2020.

[4] X. Li, J. Wu, Z. Lin, H. Liu, and H. Zha, "Recurrent squeeze-and-excitation context aggregation net for single image deraining," in *Proc. ECCV*, 2018.

[5] D. Ren, W. Zuo, Q. Hu, P. Zhu, and D. Meng, "Progressive image deraining networks: a better and simpler baseline," in *Proc. IEEE CVPR*, 2019.

[6] Y. Li and M. S. Brown, "Single image layer separation using relative smoothness," in *Proc. IEEE CVPR*, 2014.

[7] X. Fu, J. Huang, X. Ding, Y. Liao, and J. Paisley, "Clearing the skies: A deep network architecture for single-image rain removal," *IEEE TIP*, vol. 26, pp. 2944–2956, June 2017.

[8] R. Qian, R. T. Tan, W. Yang, J. Su, and J. Liu, "Attentive generative adversarial network for raindrop removal from a single image," in *Proc. IEEE CVPR*, pp. 2482–2491, 2018.

[9] W. Yang, R. T. Tan, J. Feng, J. Liu, and S. Yan, "Deep joint rain detection and removal from a single image," in *Proc. IEEE CVPR*, 2017.

(a) Rainy LFI (b) [6], 18.41/0.587 (c) [7], 17.57/0.571 (d) [8], 24.74/0.801 (e) [9], 20.03/0.820 (f) [4], 32.04/**0.955**

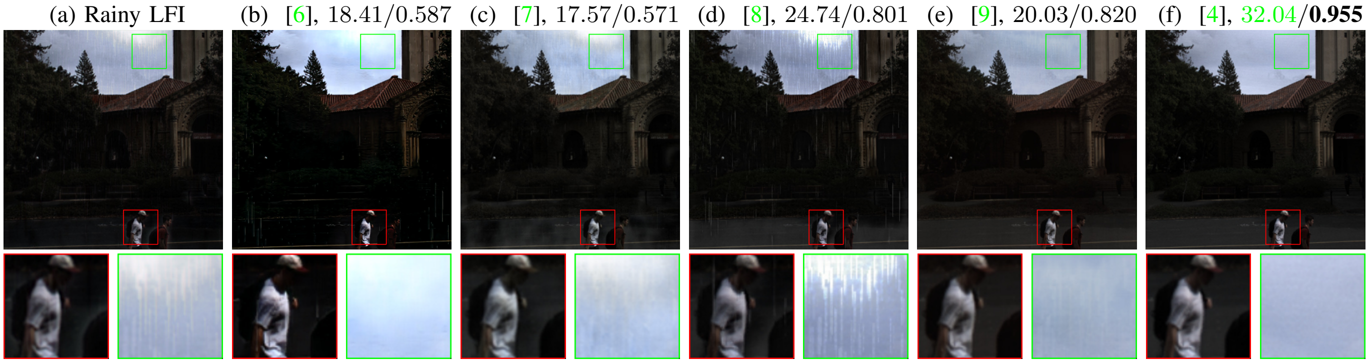

(g) [5], 27.53/0.873 (h) [1], 22.64/0.582 (i) [2], 30.33/0.928 (j) [3], 25.53/0.862 (k) Ours, **33.92**/0.943 (l) GT

Fig. 1: Comparisons of different methods for rain streaks removal on LFI. The de-rained image of each method is marked with its PSNR/SSIM values. The best value is marked in **bold**, and the second best is marked in cyan.

(a) Rainy, psnr/ssim (b) [6], 14.63/0.389 (c) [7], 13.96/0.395 (d) [8], 23.51/0.664 (e) [9], 16.54/0.629 (f) [4], 32.72/0.883

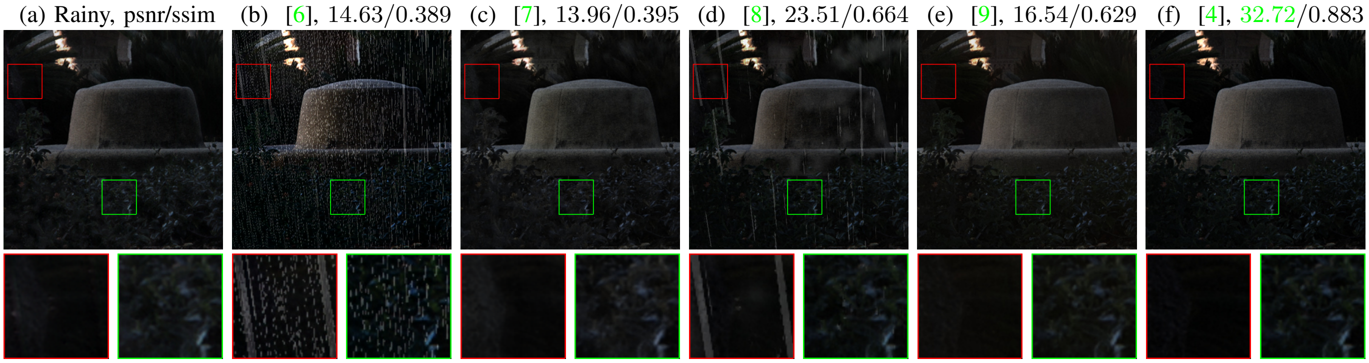

(g) [5], 30.12/0.844 (h) [1], 21.49/0.326 (i) [2], 30.47/0.844 (j) [3], 26.82/0.782 (k) Ours, **33.26**/0.895 (l) GT

Fig. 2: Comparisons of different methods for rain streaks removal on LFI. The de-rained image of each method is marked with its PSNR/SSIM values. The best value is marked in **bold**, and the second best is marked in cyan.

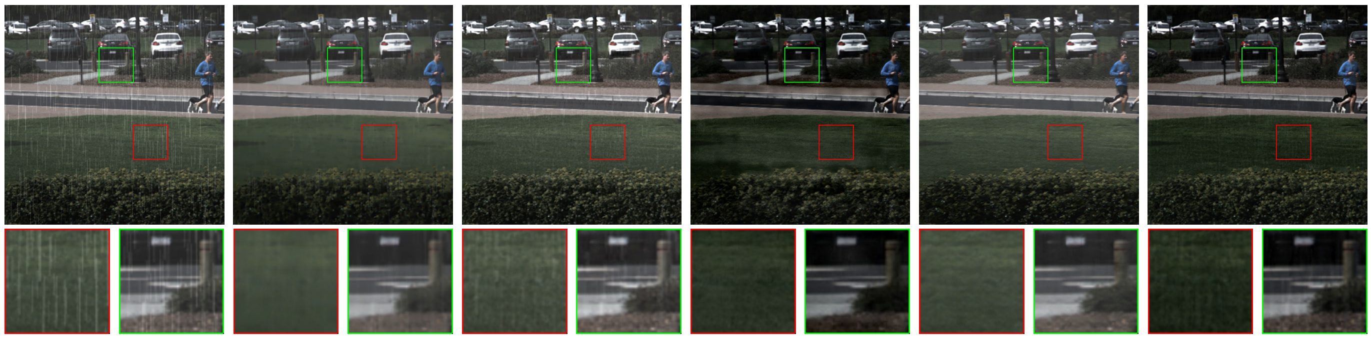

(a) Rainy, LFI (b) [6], 19.19/0.769 (c) [7], 18.11/0.784 (d) [8], 25.81/0.877 (e) [9], 20.91/0.889 (f) [4], 31.60/0.948

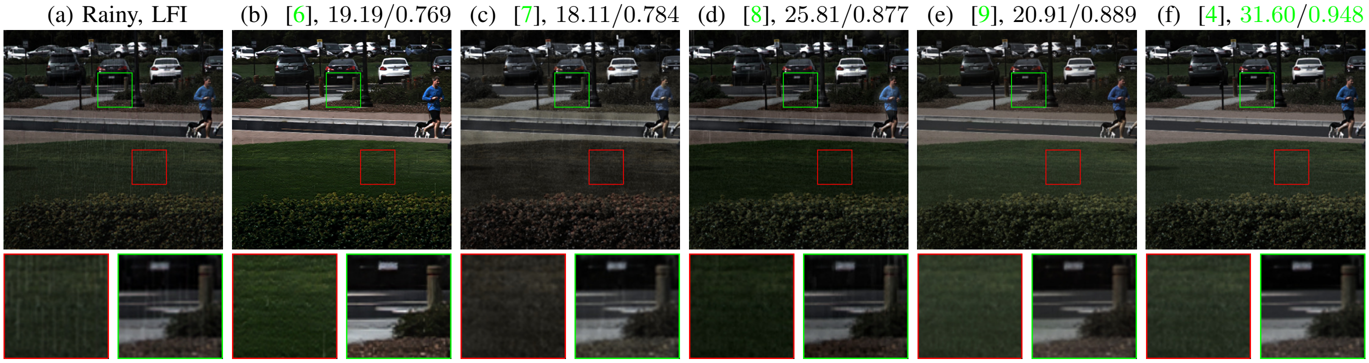

(g) [5], 28.85/0.936 (h) [1], 24.62/0.824 (i) [2], 29.83/0.908 (j) [3], 23.33/0.867 (k) Ours, **35.35**/**0.968** (l) GT

Fig. 3: Comparisons of different methods for rain streaks removal on LFI. The de-rained image of each method is marked with its PSNR/SSIM values. The best value is marked in **bold**, and the second best is marked in cyan.

(a) Rainy, psnr/ssim (b) [6], 16.28/0.491 (c) [7], 15.22/0.503 (d) [8], 26.70/0.753 (e) [9], 17.98/0.673 (f) [4], **39.03**/**0.973**

(g) [5], 34.29/0.938 (h) [1], 21.59/0.397 (i) [2], 35.87/0.960 (j) [3], 28.80/0.841 (k) Ours, 34.52/0.914 (l) GT

Fig. 4: Comparisons of different methods for rain streaks removal on LFI. The de-rained image of each method is marked with its PSNR/SSIM values. The best value is marked in **bold**, and the second best is marked in cyan.

PSNR	Fig.6a	Fig.6m	Fig.7a	Fig.11a	Fig.11m	Fig.12a	Fig.12m	Fig. 1	Fig. 2	Fig. 3	Fig. 4	Fig. 5
Li [6]	18.78	17.17	14.69	14.19	14.09	16.20	16.95	18.41	14.63	19.19	16.28	17.34
Fu [7]	17.73	16.29	14.13	13.38	13.49	15.49	15.99	17.57	13.96	18.11	15.22	16.52
Qian [8]	28.10	28.07	25.94	23.26	26.04	21.72	24.79	24.74	23.51	25.81	26.70	24.47
Yang [9]	20.44	18.80	16.26	16.27	15.76	18.31	19.09	20.03	16.54	20.91	17.98	19.50
Li [4]	35.38	**34.94**	26.02	28.52	**34.51**	20.45	34.28	32.04	32.72	31.60	**39.03**	31.30
Ren [5]	32.11	30.36	26.48	25.69	30.35	21.12	30.55	30.12	27.53	28.85	34.29	27.20
Li [1]	24.54	25.87	22.20	18.21	24.14	16.65	18.43	22.64	21.49	24.62	21.59	19.32
Wang [2]	33.34	29.99	26.65	27.87	28.39	20.94	31.22	30.33	30.47	29.83	35.87	29.44
Jiang [3]	30.60	32.19	25.90	24.03	27.35	18.92	26.61	25.53	26.82	23.33	28.80	24.82
Our's no NL	32.08	30.88	30.60	28.54	23.13	29.86	32.18	21.14	32.59	28.82	31.94	33.11
Our method	**37.64**	34.33	**33.21**	**33.15**	30.96	**34.12**	**35.62**	**33.92**	**33.26**	**35.35**	34.52	**35.58**

TABLE IV: The PSNR values of the restored LF image obtained by our method and the comparative methods [6] [7] [8] [9] [4] [1] [2] [3] as shown in Figs. The second-best values are marked as green. The figures' number marked in cyan denote resulted images exhibited in our paper, and figures' number marked in red denote resulted images exhibited in this supplementary material.

SSIM	Fig.6a	Fig.6m	Fig.7a	Fig.11a	Fig.11m	Fig.12a	Fig.12m	Fig. 1	Fig. 2	Fig. 3	Fig. 4	Fig. 5
Li [6]	0.645	0.603	0.607	0.610	0.525	0.732	0.635	0.587	0.389	0.769	0.491	0.525
Fu [7]	0.627	0.591	0.594	0.648	0.519	0.764	0.653	0.571	0.395	0.784	0.503	0.563
Qian [8]	0.866	0.883	0.850	0.794	0.831	0.768	0.796	0.801	0.664	0.877	0.753	0.691
Yang [9]	0.844	0.804	0.780	0.713	0.721	0.795	0.717	0.820	0.629	0.889	0.673	0.744
Li [4]	0.944	0.971	0.873	**0.954**	**0.961**	0.853	**0.959**	**0.955**	0.883	0.948	**0.973**	**0.949**
Ren [5]	0.911	0.923	0.891	0.912	0.922	0.861	0.923	0.873	0.844	0.936	0.938	0.875
Li [1]	0.796	0.850	0.671	0.504	0.597	0.336	0.462	0.582	0.326	0.824	0.397	0.357
Wang [2]	0.907	0.908	0.873	0.910	0.902	0.847	0.929	0.928	0.844	0.908	0.960	0923
Jiang [3]	0.889	0.929	0.856	0.828	0.839	0.744	0.843	0.862	0.782	0.867	0.841	0.771
Our's no NL	0.949	0.930	0.903	0.950	0.915	0.941	0.941	0.939	**0.905**	0.968	0.940	0.935
Our method	**0.954**	**0.955**	**0.907**	0.952	0.913	**0.944**	0.952	0.943	0.895	**0.968**	0.914	0.946

TABLE V: The SSIM values of the restored LF image obtained by our method and the comparative methods [6] [7] [8] [9] [4] [1] [2] [3] as shown in Figs. The second-best values are marked as green. The figures' number marked in cyan denote resulted images exhibited in our paper, and figures' number marked in red denote resulted images exhibited in this supplementary material.

(a) Rainy, psnr/ssim (b) [6], 17.34/0.525 (c) [7], 16.52/0.563 (d) [8], 24.47/0.691 (e) [9], 19.50/0.744 (f) [4], 31.30/**0.949**

(g) [5], 27.20/0.875 (h) [1], 19.32/0.357 (i) [2], 29.44/0.923 (j) [3], 24.82/0.771 (k) Ours, **35.58**/0.946 (l) GT

Fig. 5: Comparisons of different methods for rain streaks removal on LFI. The de-rained image of each method is marked with its PSNR/SSIM values. The best value is marked in **bold**, and the second best is marked in cyan.

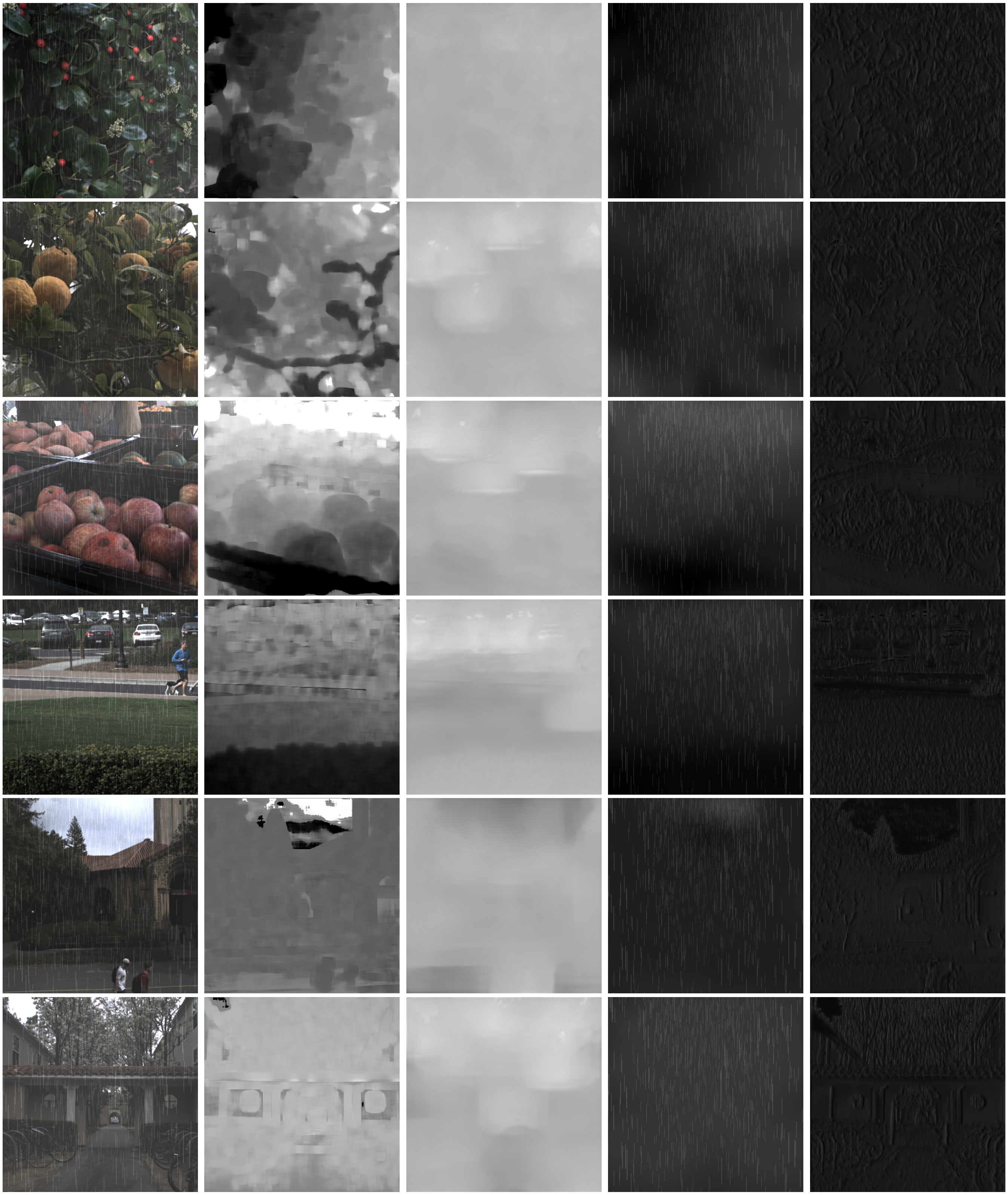

(a) input (b) depth(ours) (c) depth([1]) (d) rain-streak(ours) (e) rain-streak([1])

Fig. 6: Depth maps and rain-streak images of synthetic LFIs. In each group, (a) shows the rainy central sub-view. (b)shows depth map of central sub-view by our method. (c) shows depth map of central sub-view by [1]. (d) shows the rain-streak image of the central sub-view obtained by our method. (e) shows depth map of central sub-view by [1].

(a) input (b) depth(ours) (c) depth([1]) (d) rain-streak(ours) (e) rain-streak([1])

Fig. 7: Depth maps and rain-streak images of synthetic LFIs. In each group, (a) shows the rainy central sub-view. (b)shows depth map of central sub-view by our method. (c) shows depth map of central sub-view by [1]. (d) shows the rain-streak image of the central sub-view obtained by our method. (e) shows depth map of central sub-view by [1].

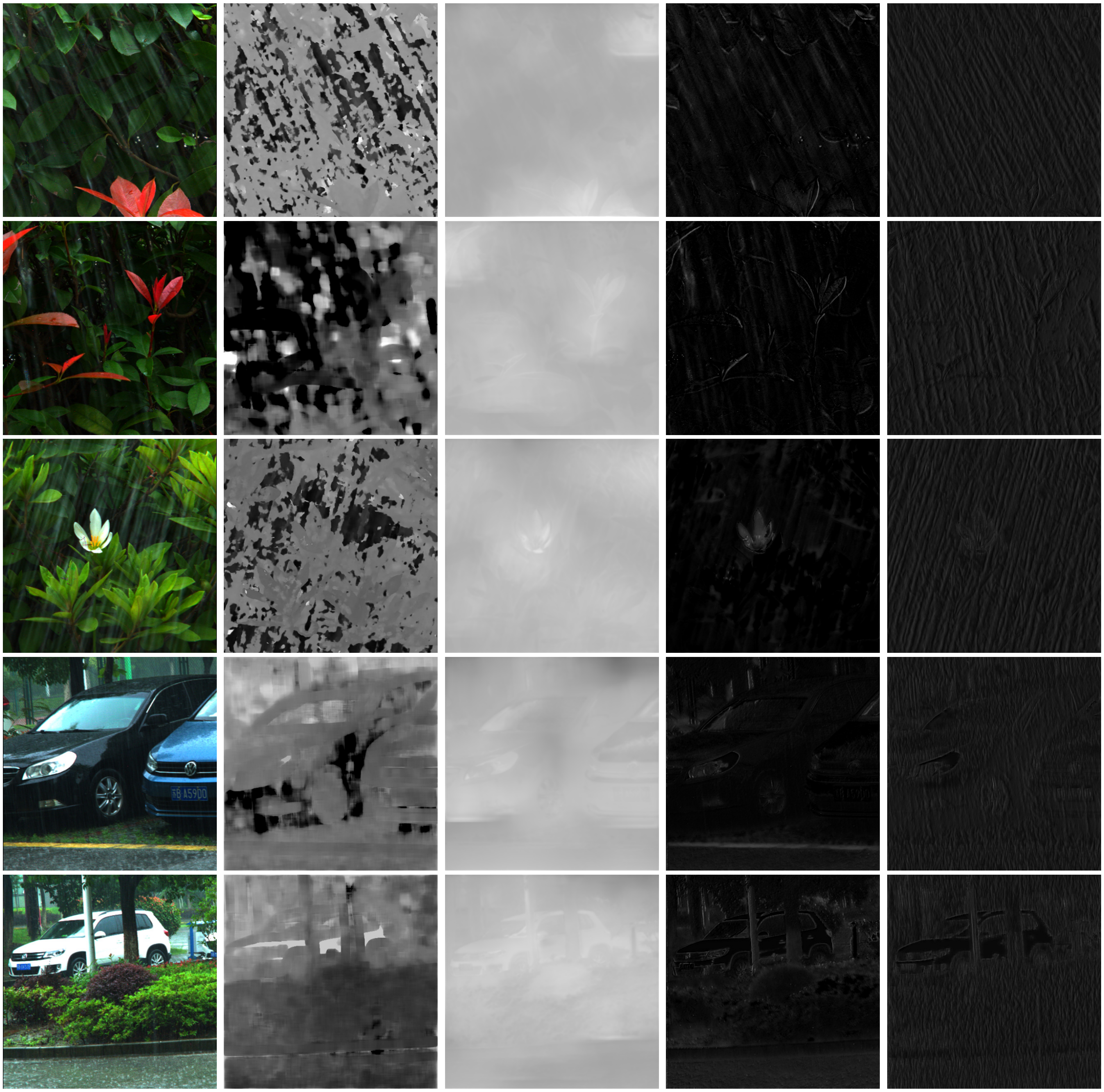

(a) input (b) depth(ours) (c) depth([1]) (d) rain-streak(ours) (e) rain-streak([1])

Fig. 8: Depth maps and rain-streak images of real LFIs. In each group, (a) shows the rainy central sub-view. (b) shows depth map of central sub-view by our method. (c) shows depth map of central sub-view by [1].(d) shows the rain-streak image of the central sub-view obtained by our method. (e) shows depth map of central sub-view by [1].

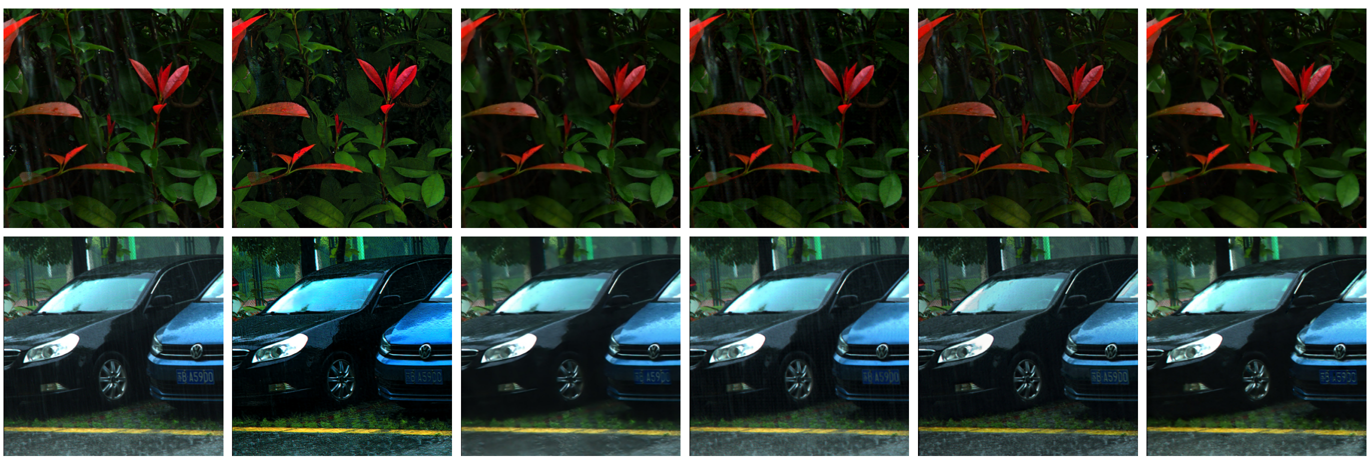

(a) Input (b) Li [1] (c) Wang [2] (d) Jiang [3] (e) Ours without DA (f) Ours

Fig. 9: Comparisons of different methods for rain-streaks removal on real-world LFIs. (e) are results of our method without domain adaption (DA) semi-supervised learning, and (f) show the results of our method with the domain adaption semi-supervised learning.

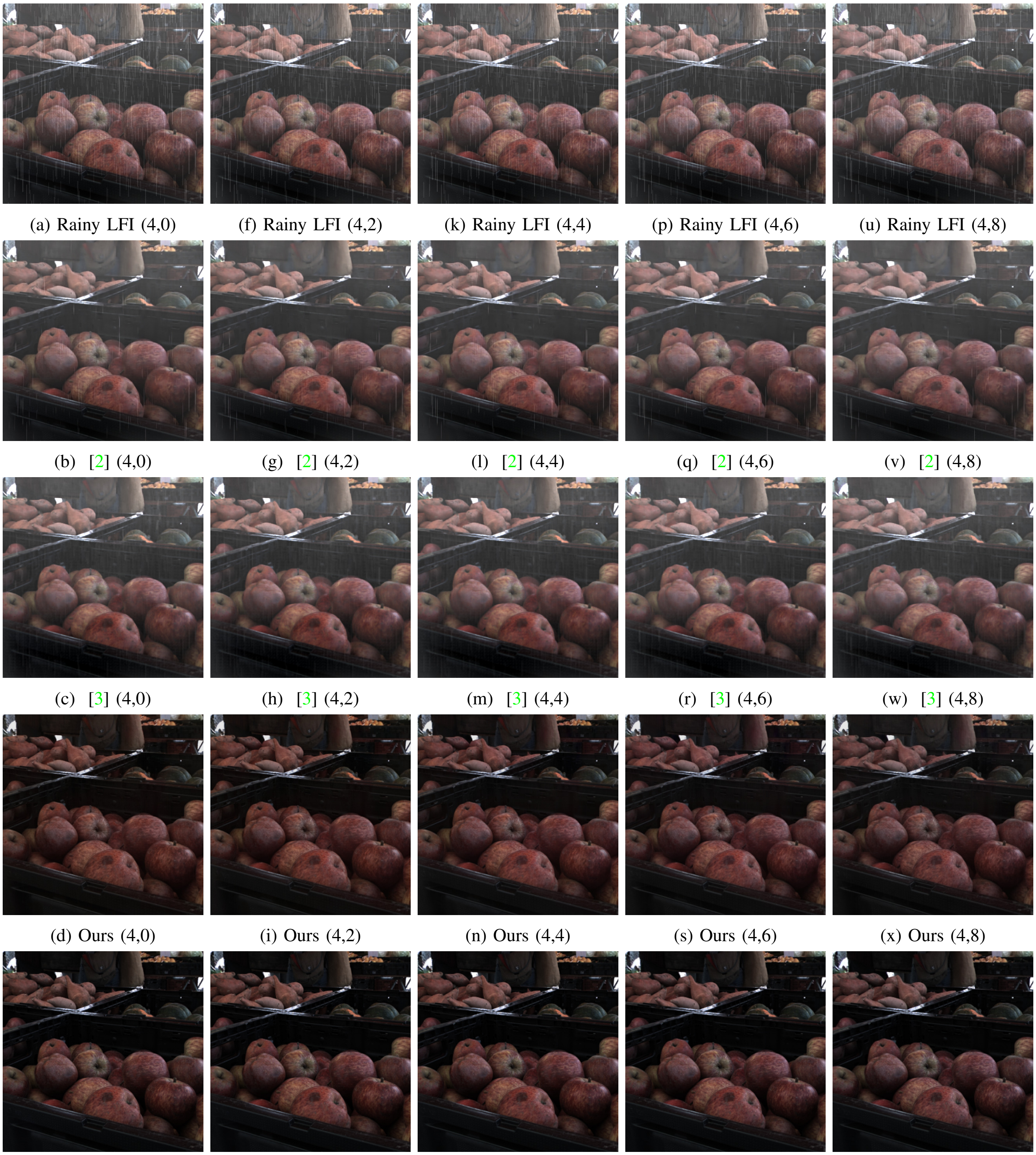

(a) Rainy LFI (4,0) (f) Rainy LFI (4,2) (k) Rainy LFI (4,4) (p) Rainy LFI (4,6) (u) Rainy LFI (4,8)

(b) [2] (4,0) (g) [2] (4,2) (l) [2] (4,4) (q) [2] (4,6) (v) [2] (4,8)

(c) [3] (4,0) (h) [3] (4,2) (m) [3] (4,4) (r) [3] (4,6) (w) [3] (4,8)

(d) Ours (4,0) (i) Ours (4,2) (n) Ours (4,4) (s) Ours (4,6) (x) Ours (4,8)

(e) GT (4,0) (j) GT (4,2) (o) GT (4,4) (t) GT (4,6) (y) GT (4,8)

Fig. 10: Selected de-rained subaperture views of the rainy LFIs obtained by our method and methods [4] [5].

(a) Rainy LFI (4,0) (f) Rainy LFI (4,2) (k) Rainy LFI (4,4) (p) Rainy LFI (4,6) (u) Rainy LFI (4,8)

(b) [2] (4,0) (g) [2] (4,2) (l) [2] (4,4) (q) [2] (4,6) (v) [2] (4,8)

(c) [3] (4,0) (h) [3] (4,2) (m) [3] (4,4) (r) [3] (4,6) (w) [3] (4,8)

(d) Ours (4,0) (i) Ours (4,2) (n) Ours (4,4) (s) Ours (4,6) (x) Ours (4,8)

(e) GT (4,0) (j) GT (4,2) (o) GT (4,4) (t) GT (4,6) (y) GT (4,8)

Fig. 11: Selected de-rained subaperture views of the rainy LFIs obtained by our method and methods [4] [5].

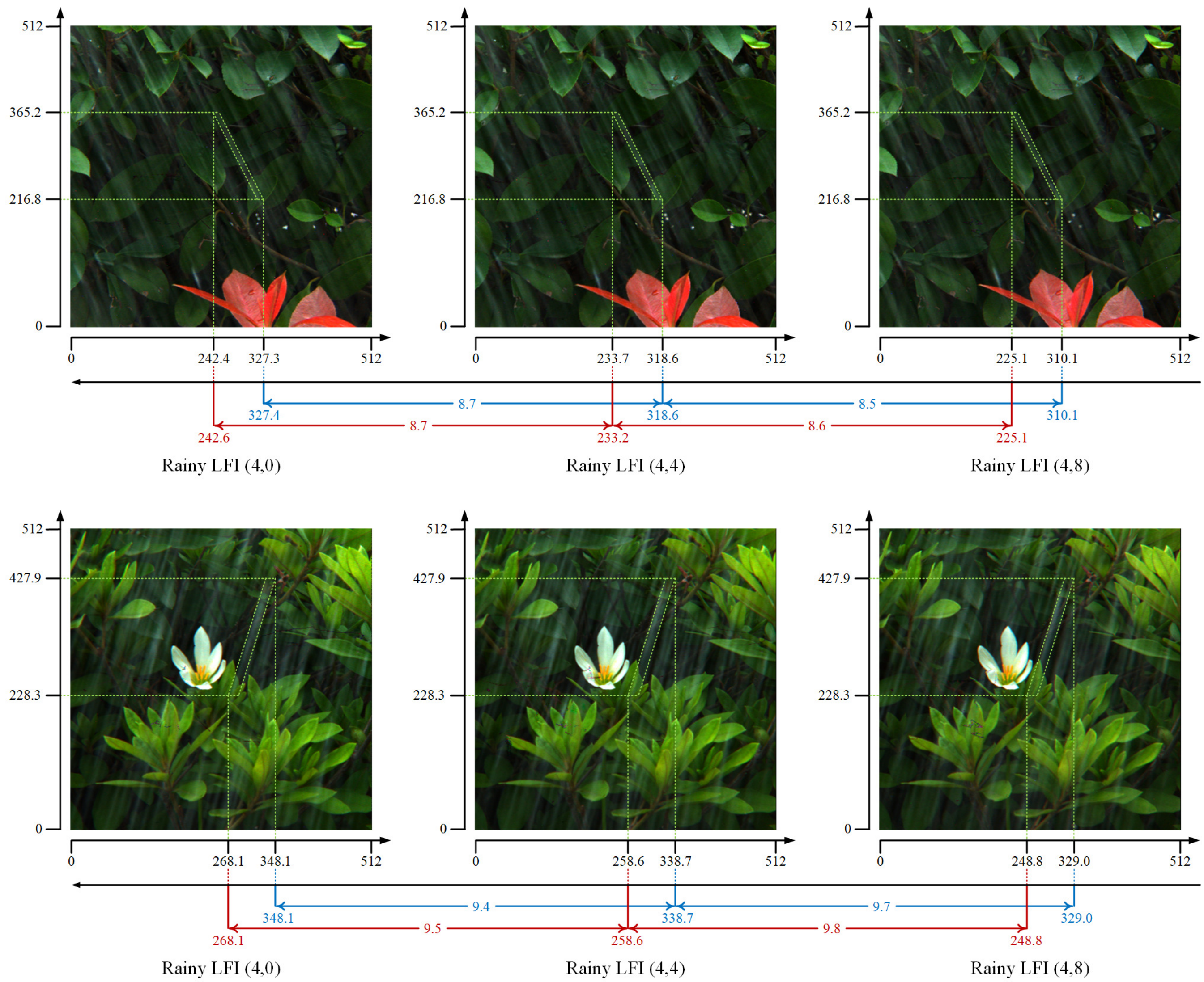

Fig. 12: Correlation of rain streaks in different sub-views, in which dashed lines indicate the coordinates (in pixel) of rain streaks in different sub-views.